A Cryogenic Rankine Cycle for Space Power Generation

Jack E. McKeathen*, Richard F. Reidy†, Sandra K. S. Boetcher‡, and Matthew J. Traum‡
University of North Texas, Denton, TX 76203-5017

Space-based Rankine cycles will someday provide high-power density and excellent thermodynamic efficiency for future space missions. However, realization of high-temperature microgravity Rankine cycles is years away. Capitalizing on existing techniques for handling low-temperature fluids in space, we propose that a *cryogenic* Rankine cycle capable of space operation be implemented using existing technology. Orientation calculations based on condensing flow through a space-borne radiator show that this cycle is both thermodynamically feasible and can produce more power than a photovoltaic array of equivalent area. Key to microgravity Rankine cycle implementation is phase separation via liquid capillarity to replace the action of gravity. Under representative conditions, fluid residence time of only 0.16 s within a porous barrier with 10 μm diameter capillaries provides adequate liquid-vapor separation in the absence of gravity. Reliance on capillarity for phase separation induces a pressure gradient within the condenser exceeding that of a normal Rankine cycle owing to Young-Laplace pressure. The appropriate fluid flow velocity derived from Washburn's equation is given. Unlike its terrestrial counterparts, the space-based cryogenic Rankine cycle will have three distinct pressure zones owing to micro-fluidic effects. The seminal work to measure cryogenic liquid contact angles occurred in the 1970s with no modern follow-up. Modern, high-resolution digital photography and computational tools can eliminate the experimental difficulties faced 30 years ago. To update the early measurements, two different experiments were attempted.

Nomenclature

A	=	condenser area
b	=	diffusion length
D_{N_2}	=	nitrogen self-diffusion coefficient
f	=	friction factor
G	=	fluid mass velocity
H_i	=	enthalpy at state i
H_{lv}	=	enthalpy of fusion
L	=	condenser length
M	=	molecular weight
$\dot{m}_t$	=	total fluid mass transfer rate
$\dot{m}_v$	=	vapor mass transfer rate
N_A	=	Avogadro's number
P	=	pressure
$P_{expander,out}$	=	expander outlet pressure
$P_{pump,in}$	=	pump inlet pressure
$\dot{q}$	=	rate of heat rejection per unit area
$\dot{Q}_{in}$	=	rate of cycle heat input
$\dot{Q}_{out}$	=	rate of cycle heat output
r	=	condenser radius
R	=	capillary radius
R_u	=	universal gas constant
T_{cold}	=	cold-side cycle temperature
T_{fluid}	=	fluid temperature
T_{hot}	=	hot-side cycle temperature
T_{space}	=	temperature of black space
t	=	time
V	=	velocity
$\dot{W}_{out}$	=	cycle power output
X	=	mixture quality
z	=	axial coordinate within condenser
δ	=	kinetic collision diameter of a molecule
$\Delta P_{condenser}$	=	pressure gradient across condenser
Δz	=	differential length within condenser
γ	=	liquid surface tension
η	=	viscosity
η_{carnot}	=	Carnot efficiency
Ξ	=	capillary volume
θ	=	contact angle
ρ	=	density
σ	=	Stefan-Boltzmann constant
τ	=	residence time

* Undergraduate Research Assistant, Mechanical and Energy Engineering Department, AIAA Student Member.
† Associate Professor, Materials Science and Engineering Department, AIAA Member.
‡ Assistant Professor, Mechanical and Energy Engineering Department, 1155 Union Circle #311098 Denton, Texas 76203-5017, AIAA Member.

I. Introduction

The unique surface affinity of cryogenic liquids to solid surfaces can provide simultaneous phase separation and heat transfer within the condenser stage of a space-based Rankine cycle. Working microgravity Rankine cycle technology is identified by NASA as an essential element for future space missions to provide high-power density and superior thermodynamic efficiency[1] compared to existing space-based energy generation methods.[2] Initial theoretical design of a terrestrial cryogenic Rankine cycle has already been completed,[3] and ground-based cryogenic Brayton cycles have been successfully demonstrated.[4,5,6] Figure 1 shows the essential components of an idealized Rankine cycle.

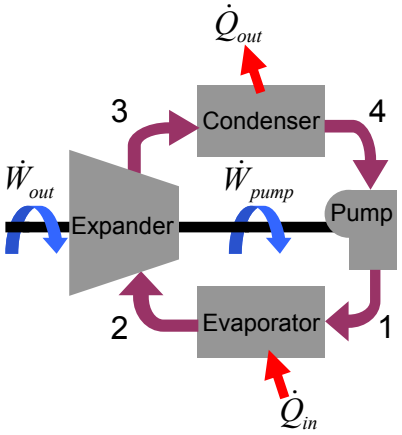

Figure 1. Essential components and process stages of an idealized Rankine cycle.

In conventional terrestrial applications, Rankine-cycle power plants achieve working fluid phase separation through buoyancy. However, in a microgravity environment, the gas phase does not spontaneously rise from the liquid, and phase change must be accomplished through alternative methods. Research on phase separation of microgravity cryogenic fluid with porous barriers has been conducted.[7] Both the U.S. military and NASA have pioneered separation and management of cryogenic fluids for space flight functions including fuel management, life support, and supply transfer.[8,9] Terrestrial research has demonstrated the fundamentals for two-phase heat transfer in cryogenic fluids.[10,11].

Previous microgravity cryogenic fluid phase separators utilized the super-fluid properties of helium II by capitalizing upon the thermomechanical effect across a porous plug to separate liquid from gas.[12,13,14] Certain types of porous plugs are also efficient microgravity phase separators for helium I, which is not a superfluid.[15] Thus, phase separation of other cryogenic fluids, such as liquid nitrogen, can be achieved by applying findings demonstrated for helium I. However, underlying thermal-fluidic parameters of these fluids, such as contact angle, density, surface tension, and viscosity must be accurately known to design porous barrier phase separators that will perform as desired.

In this paper we present an orientation calculation to size a space-based cryogenic Rankine cycle with respect to conventional photovoltaic (PV) arrays which are now in use for on-orbit power generation. We then provide design calculations describing how porous barriers can facilitate microgravity phase separation in a condenser. Finally, we conclude with descriptions of attempted techniques to measure the liquid nitrogen static contact angle on metal substrates. While it turns out that precise measurement of contact angle is not critical to condenser design, the knowledge and experimental infrastructure created through successful contact angle measurement are preliminary steps to help predict behavior of micro-gravity condensing flow within porous barriers.

II. Background

Since capillary action replaces gravity for phase separation in a space-based Rankine cycle, details of how cryogenic fluid behaves in capillaries is necessary to characterize cycle function. Thus, the preliminary parameter to examine is the static contact angle liquid nitrogen makes with metals from which the condenser will likely be made. The literature is inconsistent on the static contact angle of liquid nitrogen with solid metal substrates. Grigor, Pavlov, and Ametistov[16] provide indirect evidence that the contact angle approaches 0°. They postulate a model for cryogenic boiling bubble formation predicated on thin liquid film continuously filling the nucleation site during bubble formation. This process is enabled through capillary wicking arising from 0° contact angle. They successfully superimpose their model on prior vapor bubble growth data for surfaces of copper, nickel, and steel. However, they state that the experimental data and their model remain in agreement for contact angles up to 54°, leaving enormous uncertainty in the correct parameter value.

Using the tilting plate method, Brennen and Skrabek[17] measured a range of 7.0° to 9.0° for nitrogen on aluminum via the most careful, thorough, and well-described approach in the literature. Using a range of temperatures, they tried many surfaces made from a variety of chemicals coated on metal substrates. They also collected data for uncoated aluminum at 79.5 K, but no additional metals or temperatures were explored. Brennen and Skrabek report that for angles smaller than 10.0°, interference from light reflections used to take the measurements compounded with liquid surface movement confounded the measurements' accuracy. Moreover, small angles magnified errors in the reference establishment process, most notably backlash in the gear system. So, these results could be further improved with modern techniques and equipment.

Like Grigor, Pavlov, and Ametistov, Bald[18] uses a bubble formation argument to estimate liquid nitrogen's contact angle. He incompletely cites the experimental observations of Brennen and Skrabek, giving 7.0° for aluminum substrates. Bald also cites apparently unpublished work by Bland,[19] in which bubble formation during cryogenic boiling was directly observed. However, Bald gives no numerical values arising from Bland's work.

The largest liquid nitrogen contact angle value reported in the literature, 13.75°, is given by Steiner and Schlunder[20] who, like Grigor, Pavlov, and Ametistov, used liquid nitrogen boiling processes to infer contact angle. However, these researchers use their own data instead of borrowing existing literature results.

All of these manuscripts were prepared in the 1970s with no modern follow-up work reported. Even the praiseworthy method of Brennen and Skrabek was subject to uncertainties that can today be eliminated by modern, high-resolution digital photography and computer-controlled actuators. We thus have an opportunity to update these early measurements for a range of relevant metal substrates and operating temperatures by using digital imaging coupled with computational tools unavailable in the 1970s.

III. Modeling

To determine feasibility of deploying a cryogenic Rankine cycle in space, we compare it on a power-to-area ratio basis against the recently deployed S6 3B photovoltaic wings on the International Space Station (ISS). The ISS S6 3B wings have an area of 892 m^2, and they generate 15 peak kilowatts,[21] giving a power-to-area ratio of 16.8 W/m^2 at peak output. Unlike PV, a Rankine cycle can operate continuously at peak power in sunlight, shadow, or in deep space. Nonetheless, PV peak output is used as the benchmark for this orientation calculation. Heat and entropy rejection at the Rankine cycle condenser necessitate a significant radiator surface area, making the condenser the largest cycle component. Thus, the condenser is used to estimate physical size of the cycle. While sophisticated analysis of microgravity two-phase flow[22] and condensing flow[23] exist in the literature, we adopt a simple model for orientation calculation purposes. This analysis begins by first applying the Carnot cycle approximation and the First Law of Thermodynamics to the entire Rankine cycle.

$$1 - \frac{T_{cold}}{T_{hot}} = \eta_{carnot} = \frac{\dot{W}_{out}}{\dot{Q}_{in}} \tag{1}$$

$$\dot{Q}_{in} = \dot{W}_{out} + \dot{Q}_{out} \tag{2}$$

Given the operating temperatures, T_{cold} and T_{hot}, the required heat rejection is calculated via the enthalpy change between State 3 (saturated vapor) and 4 (saturated liquid) for nitrogen (see Fig. 1). Please note that T_{cold} is the fluid temperature.

$$\dot{Q}_{out} = \dot{m}_t\left(H_4(T_{fluid}) - H_3(T_{fluid})\right) = \dot{m}_t H_{lv}(T_{fluid}) \tag{3}$$

Combining Eqs. (1) – (3) gives an expression for mass transport rate through the condenser.

$$\dot{m}_t = \frac{\left(\frac{T_{fluid}}{T_{hot}}\right)\dot{W}_{out}}{H_{lv}(T_{fluid})\left(1 - \frac{T_{fluid}}{T_{hot}}\right)} \tag{4}$$

It is assumed that the exterior wall of the condenser/radiator is thin (i.e., supporting no temperature gradient), and it radiates as a black body to black space, which is assumed to be at 4 K. Near-black-body performance can be achieved by deposition of a thin black coating on the radiator, perhaps graphite or carbon nanotubes. In addition, the temperature of the working fluid just inside the wall is also fixed because the fluid is undergoing phase change. The temperature of this phase change process, a variable to be determined in this calculation, can be fixed mechanically (or modulated as needed) by appropriate selection of the Rankine cycle pump setting.

The dominant variable in condensing internal flows is the mixture quality *X(z)* which is defined as the ratio of vapor mass to total flow mass at any axial station *z* down the condenser. The fluid starts as a saturated vapor at the condenser entrance ($X = 1$, $z = 0$) and exits as a saturated liquid ($X = 0$, $z = L$). Mixture quality is defined as follows,

$$X(z) = \frac{\dot{m}_v(z)}{\dot{m}_t} \tag{5}$$

By applying the continuity equation to a control volume of length Δz within the condenser, an expression for mixture quality with respect to axial location downstream in the condenser is derived.

$$\frac{\partial \mathrm{X}}{\partial \mathrm{z}} = \frac{\partial}{\partial \mathrm{z}}\left(\frac{\dot{\mathrm{m}}_{\mathrm{v}}}{\dot{\mathrm{m}}_{\mathrm{t}}}\right) = \frac{1}{\dot{\mathrm{m}}_{\mathrm{t}}}\frac{\partial \dot{\mathrm{m}}_{\mathrm{v}}}{\partial \mathrm{z}} \tag{6}$$

The heat loss from this control volume by radiation dictates how much fluid is converted from vapor to liquid at each axial location. Expressions for the heat transfer rate and mass transfer are given in Eqs. (7) and (8).

$$\dot{\mathrm{q}}(\Delta \mathrm{z} 2\pi \mathrm{r}) = \mathrm{H}_{\mathrm{lv}}(\mathrm{T}_{\mathrm{fluid}})[\dot{\mathrm{m}}_{\mathrm{v}}(\mathrm{z}) - \dot{\mathrm{m}}_{\mathrm{v}}(\mathrm{z} + \Delta \mathrm{z})] \tag{7}$$

$$-\frac{\partial \dot{\mathrm{m}}_{\mathrm{v}}}{\partial \mathrm{z}} = \frac{\dot{\mathrm{q}} 2\pi \mathrm{r}}{\mathrm{H}_{\mathrm{lv}}(\mathrm{T}_{\mathrm{fluid}})} \tag{8}$$

The heat loss from this control volume by radiation is estimated using the Stefan–Boltzmann Equation (recalling the assumption that the condenser and space both function as black bodies).

$$\dot{q} = \sigma\left(T_{fluid}^4 - T_{space}^4\right) \tag{9}$$

Combining Eqs. (6) – (9) and integrating gives the desired expression for mixture quality as a function of axial location within the condenser.

$$\int_1^{\mathrm{X}} \mathrm{dX} = -\frac{\dot{\mathrm{q}} 2\pi \mathrm{r}}{\dot{\mathrm{m}}_{\mathrm{t}} \mathrm{H}_{\mathrm{lv}}(\mathrm{T}_{\mathrm{fluid}})} \int_0^{\mathrm{z}} \mathrm{dz} \tag{10}$$

$$X = 1 - \frac{2\pi \mathrm{rz}\left[\sigma\left(T_{fluid}^4 - T_{space}^4\right)\right]}{\dot{\mathrm{m}}_{\mathrm{t}} \mathrm{H}_{\mathrm{lv}}} \tag{11}$$

Recognizing the quantity ($2\pi rz$) as the condenser area A and inserting Eq. (4) into Eqs. (10) and (11) gives the desired expression.

$$X = 1 - \frac{\mathrm{A}\left[\sigma\left(T_{fluid}^4 - T_{space}^4\right)\right]\left[1 - \frac{T_{fluid}}{T_{hot}}\right]}{\left(\frac{T_{fluid}}{T_{hot}}\right)\dot{\mathrm{W}}_{\mathrm{out}}} \tag{12}$$

The final step is to solve Eq. (12) to find the fluid temperature required for the condenser to convert all vapor to liquid (corresponding to $X = 0$) for a particular power-to-area ratio. It is desirable for the cycle to achieve a power-to-area ratio meeting or exceeding the 16.8 W/m^2 realized by the ISS PV array.

$$\frac{\dot{\mathrm{W}}_{\mathrm{out}}}{A} = \frac{\left[\sigma\left(T_{fluid}^4 - T_{space}^4\right)\right]\left[1 - \frac{T_{fluid}}{T_{hot}}\right]}{\left(\frac{T_{fluid}}{T_{hot}}\right)} \tag{13}$$

Figure 2 shows curves from Eq. (13) representing power-to-area ratio as a function of fluid temperature ranging over the entire two-phase region for nitrogen. A variety of evaporator temperatures T_{hot} are plotted from 300 K to 600 K in increments of 100 K. As expected, the power-to-area ratio of the cryogenic Rankine cycle increases as the evaporator temperature gets hotter owing to the innate increase in cycle thermodynamic efficiency. Importantly, for evaporator temperatures of 300 K and higher, cryogenic Rankine cycle power-to-area ratio meets or exceeds the ratio for PV arrays for condenser temperatures above 118 K. This analysis demonstrates two key points. First, cryogenic Rankine cycles are feasible under these conditions because 118 K is below the nitrogen critical point at 127 K. Thus, liquid (and not supercritical fluid, which will not phase separate) can be produced in the condenser.

Second, a space-based cryogenic Rankine cycle can produce more power than a PV array of equivalent area. Nonetheless, this technology is not intended to be a long-term replacement for PV arrays for space power. Instead it is intended to demonstrate near-term viability of orbiting low-temperature Rankine cycles for research and power production to stimulate and motivate development of high-temperature cycles with even better thermal efficiency.

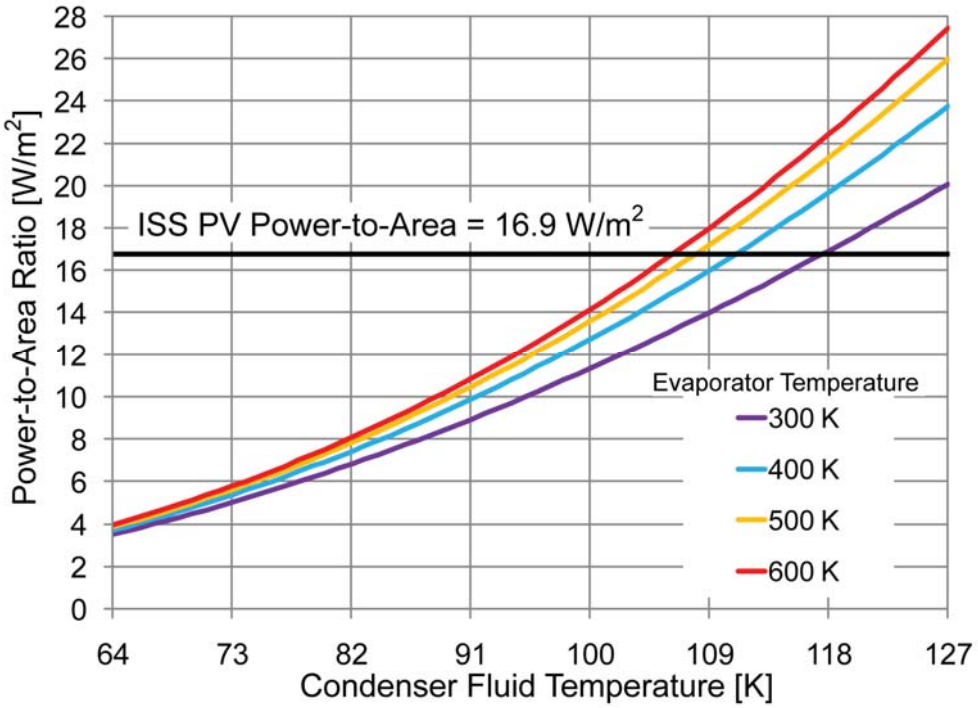

Figure 2. Cryogenic Rankine cycle power-to-area ratios as a function of condenser temperature for a range of evaporator fluid temperatures from 300 K to 600 K. Above a condenser fluid temperature of 118 K, the cycle power-to-area ratio exceeds that of conventional PV arrays, and it continues to improve as cycle efficiency increases with higher evaporator temperature.

Of course, high pressure is required to liquefy nitrogen at 118 K, but the high-pressure requirement becomes less severe as the condenser temperature falls. For the analyses that follow, a condenser temperature of 106 K is selected. This state corresponds to 1.15×10^6 Pa nominal condenser pressure realized at an evaporator temperature of 600 K with a power-to-area ratio matching the ISS PV array: 16.8 W/m^2. Applying Eq. (1), the thermodynamic efficiency for this cycle approaches 82% with a requirement to reject 0.18 kW heat for each 1 kW of power generated. Eq. (3) indicates need for a working fluid mass flow rate of 0.00123 kg/s per 1 kW of power generated under these conditions.

The key to microgravity Rankine cycle operation is phase separation in the condenser to assure that only liquid is delivered to the pump. An important motivation for using cryogenic fluid in this space-based two-phase power cycle is high surface affinity of cryogenic liquids to surfaces. Capillary-filled porous barriers used in the condenser provide large surface area to promote liquid-wall adhesion. Condensate should form on the pore walls because heat is extracted from the two-phase flow at this surface. Moreover, walls contain intrinsic surface roughness that seeds formation of liquid. Nonetheless, if vapor does spontaneously liquefy at the condenser center, Brownian motion assures that wayward liquid droplets strike a nearby wall before exiting the condenser. Thus, a porous barrier within the condenser will serve as a natural phase separator.

To estimate the required residence time τ within a porous barrier before a liquid droplet strikes a wall, the nitrogen self-diffusion coefficient D_{N_2}, at 106 K is estimated using the Chapman-Enskog equation derived from kinetic theory.[24]

$$\mathrm{D_{N_2}} = \frac{1}{3\pi^{\frac{3}{2}}} \frac{(\mathrm{R_u T_{fluid}})^{\frac{3}{2}}}{\mathrm{N_A}\delta^2 \mathrm{M}^{\frac{1}{2}} \mathrm{P}} \tag{14}$$

Values are selected to correspond with saturated nitrogen vapor in the condenser. For this calculation, the kinetic collision diameter of a nitrogen gas molecule δ is assumed to be 3.70 x 10^{-10} m.[25] These conditions give D_{N_2} = 6.33 10^{-10} m^2/s. The diffusion length $b = \sqrt{D_{N_2}\tau}$ which arises from the similarity solution to the mass diffusion equation represents how far a particle travels in time τ. The distance from a capillary tube center to its wall (i.e., the radius R) is the farthest radial distance a liquid droplet would have to travel to adhere to a surface. Thus the diffusion length can be recast to approximate a droplet residence time before striking a wall

$$\tau = \frac{1}{D_{N_2}}\left(\frac{R}{2}\right)^2 \tag{15}$$

Provided nitrogen undergoing phase change stays in the capillary at least for the duration of τ, diffusion in the radial direction assures liquid droplets forming at a capillary's center just as the fluid enters the channel will strike a wall before exiting so that only liquid emerges from the condenser at the pump inlet. To provide orientation, for a porous barrier of capillaries with pore diameter of 10 μm, the residence time is 0.16 s. If the condenser were a single long tube 1 cm in diameter, a porous barrier 0.4 mm thick inserted at the location where $X = 0$ would provide the requisite phase separation residence time. The thickness of this barrier is an important parameter because viscous losses and capillary forces in the pores retard flow in the desired direction, requiring more pumping power to circulate fluid than in a conventional Rankine cycle. It is therefore desirable to make the barrier as thin as possible while providing enough length for complete phase separation.

To calculate flow velocity in a capillary, the Washburn equation, shown in Eq. (16), applied to the flow geometry in Fig. 3 describes dynamic two-phase flow in a capillary tube.[26] A simplified form of this equation arises from the following assumptions: 1) the capillary is of constant cross sectional area, 2) the capillary contains fully-developed laminar flow with negligible flow development length, 3) the flow is homogenous [i.e., both phases move at the same velocity], and 4) the no-slip condition applies at the walls, which is a good approximation for capillaries larger than 1 μm.[27]

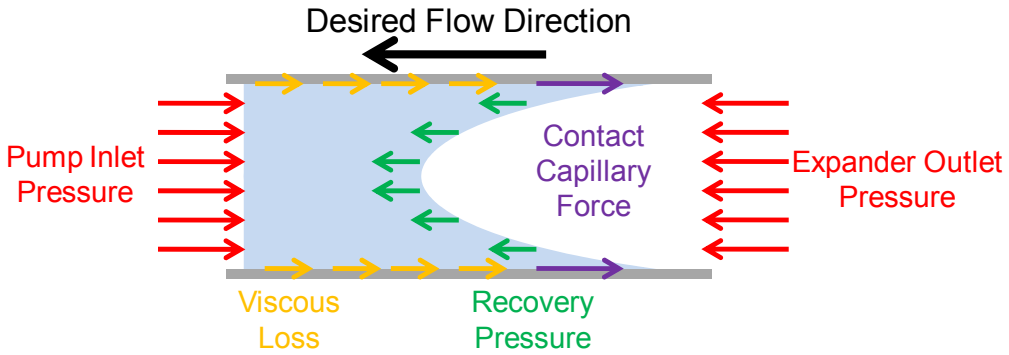

Figure 3. Force diagram showing dominant pressures and forces acting on a two-phase, microgravity, capillary flow within the condenser stage of a cryogenic Rankine cycle.

$$d\Xi = \frac{\pi \int_0^L \sum \frac{dP}{dz} dz}{8\eta L} R^4 dt \tag{16}$$

Recognizing that for a capillary of circular cross section, $d\Xi = \pi R^2 dL$, Eq. (16) can be simplified to the following form

$$\frac{dL}{dt} = V = \frac{\int_0^L \sum \frac{dP}{dz} dz}{8\eta L} R^2 \tag{17}$$

To complete the analysis, the terms making up the sum of pressures acting on the flow must be identified. In terrestrial capillary flow, hydrostatic pressure head is often dominant and cannot be ignored. However, in microgravity, hydrostatic pressure terms are negligible compared to other system pressures. Pressure loss from viscous dissipation is an important mechanism, especially through small capillaries. Unique to condensing flow is the so-called *pressure recovery term*, which arises due to decreasing momentum as working fluid transitions from gas to liquid. Finally, the capillary force at the liquid-wall contact creates a Young-Laplace pressure maintained across the liquid meniscus. Thus, the sum of pressures acting on the capillary fluid reduces to the following equation

$$\int_0^L \sum \frac{dP}{dz} dz = P_{expander,out} - P_{pump,in} - \frac{2\gamma\cos\theta}{R} + \int_0^L \left[\left(\frac{G}{\rho(z)} \right)^2 \frac{d\rho(z)}{dz} - \frac{f}{4R} \frac{G^2}{\rho(z)} \right] dz \tag{18}$$

Noting that the quantity $P_{expander,out} - P_{pump,in}$ is the mechanical pressure gradient that must be maintained across the condenser to assure fluid moves in the desired direction, Eq. (18) may be written as

$$V = \frac{R^2}{8\eta L} \left(\Delta P_{condensor} - \frac{2\gamma\cos\theta}{R} + \int_0^L \left[\left(\frac{G}{\rho(z)} \right)^2 \frac{d\rho(z)}{dz} - \frac{f}{4R} \frac{G^2}{\rho(z)} \right] dz \right) \tag{19}$$

Eq. (19) describes the parameters required to realize a desired flow velocity in the condenser. One unique attribute of a micro-gravity Rankine cycle condenser containing a porous barrier for phase separation is that the condenser itself must maintain a pressure gradient in excess of the viscosity-derived pressure drop and recovery pressure normally associated with internal condensing flow. Thus, instead of operating in the low pressure / high pressure dichotomy of a conventional Rankine cycle, the cycle described here will have three distinct pressure zones. The lowest pressure will occur at the pump inlet (Fig. 1, State 4). The highest pressure will be at the pump outlet (Figure 1, State 1) and through the evaporator (Fig. 1, State 2), and the cycle's medium pressure will be at the expander outlet (Fig. 1, State 3) entering the condenser.

IV. Experimental Description and Results

Fortunately, exact contact angle measurement is not critical when designing cryogenic Rankine cycle condenser porous barriers. As is shown in Eq. 19, contact angle is only weakly coupled to key cycle performance parameters like flow velocity and pressure because the value is known to be small and it enters in as a cosine expression. Nonetheless, due to its relative ease of measure, reliable characterization of contact angle for static liquids is a logical first step toward deeper understanding of more complex flow dynamics for this system.

Several methods are illuminated in the Background section to measure or infer contact angle of cryogenic liquid on a solid surface: the tilting plate method, direct observation of bubble formation during boiling, or indirect inference based on rates of boiling bubble formation. However, the most common approach for contact angle measurement of conventional, room temperature liquids is the so-called static sessile drop method. Figure 4 shows a typical sessile drop apparatus, which uses a syringe needle to deposit liquid droplets on a substrate. Thus, before attempting a more exotic approach, we tried to reproduce the static sessile drop method for cryogenic nitrogen.

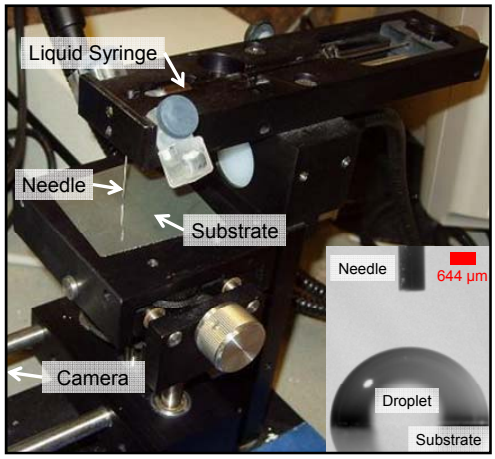

Figure 4. A conventional apparatus to measures liquid contact angles on solid surfaces via the static sessile drop method under ambient conditions.

Figure 5 shows the experimental set-up, which included a syringe filled with LN_2 sitting in an insulating Styrofoam cup that was also filled with LN_2. Nitrogen boiling away from the cup assured isothermal conditions were maintained for the liquid in the syringe. A hypodermic needle affixed to the syringe was poked through the bottom of the Styrofoam cup to mimic the needle in a conventional sessile drop apparatus. The penetration point was sealed top and bottom with vacuum grease that froze solid at cryogenic temperature to seal out leakage through the hole. This assembly was elevated on a ring stand so it hovered over a second

LN_2 reservoir within the cut out bottom of a second insulating Styrofoam cup.

A right cylinder of stainless steel which served as the stage upon which droplets were deposited was placed within the second cryogenic isothermal reservoir. Had this approach worked, the stainless steel would have later been replaced by well-characterized brass when measurements were taken. A T-type thermocouple was soldered to the bottom edge of the metal cylinder to record temperature during the process using an Omega OM-2041 portable handheld data logger. The Biot number calculated for this configuration indicated uniform temperature throughout the cylinder, signifying that the thermocouple reader represented the temperature of the metal surface where droplet deposition occurred.

The syringe was actuated manually by tapping lightly on the plunger with a gloved finger while a digital video recorder zoomed and focused on the metal surface captured droplet deposition. Still images are processed using a software-based gionometer.

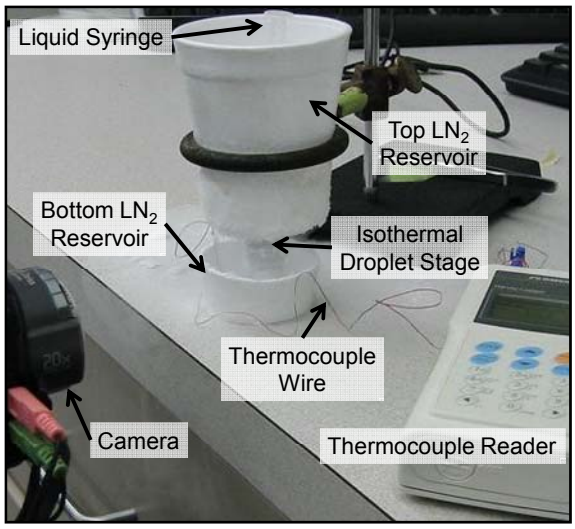

Figure 5. Reproduction of the static sessile drop method for contact angle measurement of cryogenic liquid nitrogen on a metal stage.

While the apparatus in Fig. 5 did yield droplet images, this data was not useful in determining contact angle for several reasons. First, the syringe could not be actuated delicately enough to create controlled individual droplets. Second, immediately upon pouring LN_2 into the bottom reservoir to chill the metal stage, condensation (likely water vapor) solidified on the metal from the atmosphere, fouling the droplet stage. Third, a condensate mist formed in the vicinity of the lower reservoir obscuring the camera shot, making it difficult to see the droplets. Fourth, despite the stage being chilled to LN_2 temperature, as indicated by the thermocouple reader, it appeared that nitrogen droplets began film boiling when deposited on the surface. This observation indicates a slight elevation above the boiling temperature. The film layer under the droplets invalidates the measurement method because a perfect solid-liquid interface is needed for the stationary sessile droplet approach.

Since the apparatus in Figure 5 proved unsuccessful in generating the desired contact angle data, we pursued an alternative approach: condensing liquid nitrogen on a chilled plate from an environment of pure nitrogen gas, the so-called *droplet condensation method*. An experimental apparatus, represented schematically in Fig. 6 and pictured in Fig. 7, was built to make this measurement. As shown in Fig. 6, environmental gas composition local to two cooled surfaces was controlled by evacuating a sealed bag surrounding the apparatus with a vacuum pump and filling it with gaseous nitrogen at 1 atm pressure. Liquid nitrogen below the condensation temperature of nitrogen gas was extracted from a conventional Dewar using a vacuum pump to lower its pressure. This process reduced the nitrogen boiling point and dropped the temperature below 77 K. A heat exchanger with the low-pressure (~ 0.76 atm), low-temperature (~ 75 K) liquid nitrogen running through it was placed in good thermal contact with lapped metal plates, oriented vertically and horizontally.

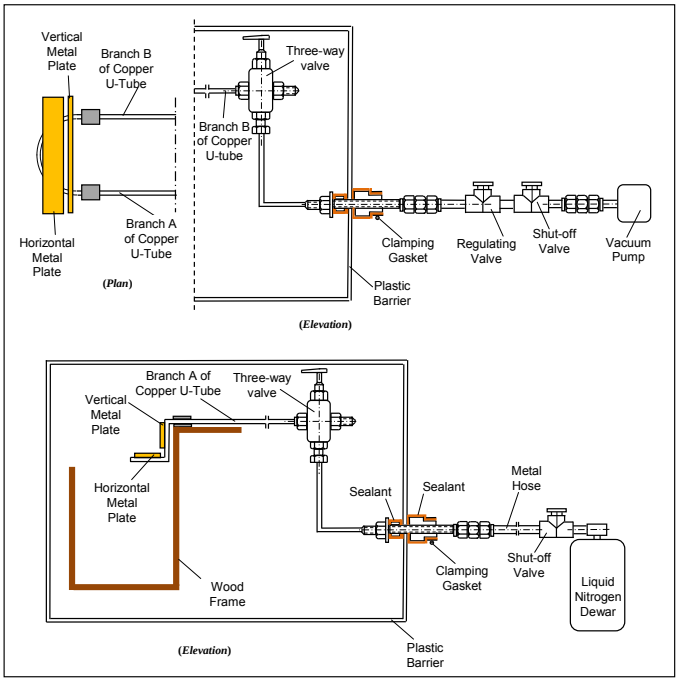

Figure 6. Schematic of the apparatus to measure liquid nitrogen contact angles on metal surfaces via the droplet condensation method. By sealing the sample in a pure gas environment, surface fouling from atmospheric contaminants was reduced.

It was expected that liquid viable for imaging

would condense on the plates by forming tiny droplets that coalesced into larger droplets, which could then be photographed using a high-resolution digital camera on high zoom for computer analysis.

The plates were specially prepared and characterized for high-quality measurements. Each plate was an Alloy 360 brass rectangle, which was machine-lapped on its exposed face using an Allied TechPrep™ automatic polishing center to achieve a mirror finish. After sample polishing, a Microphotonics Nanovea PS50 optical profiler measured an arithmetic mean surface roughness of 0.084 µm. Nonetheless, scratches and roughness features persisted. Figure 8 shows the roughest portion of the sample's profilometry profile, which includes a prominent scratch.

Unfortunately, the experiment was not well-insulated from the environment. The low-temperature heat exchanger, instrumented with an E-type thermocouple monitored by an Extech EA15 thermocouple reader, attained a temperature of only 133.5 K (Fig. 7 – Inset) against a background environment of 296 K. This coldest achieved temperature is well above the 75 – 77 K required to condense liquid nitrogen onto the interrogation surfaces at atmospheric pressure.

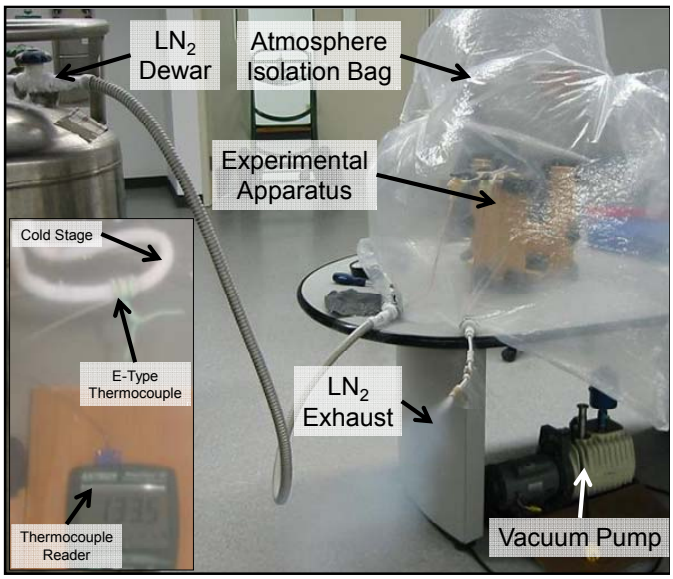

Figure 7. Apparatus to measure liquid nitrogen contact angles on metal surfaces via the droplet condensation method. (Inset) due to poor insulation from the environment, the apparatus could not cool down to 75 - 77 K, the temperature required for nitrogen condensation at ambient pressure.

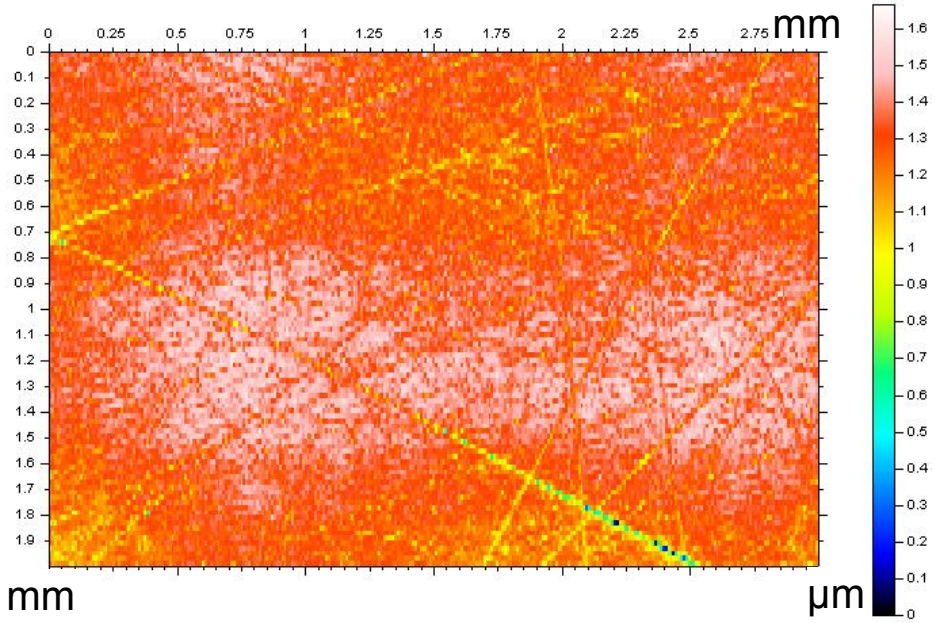

Figure 8. White light profilometry profile of a machine-lapped Alloy 360 brass plate upon which liquid nitrogen contact angle as to be measured. Arithmetic mean surface roughness is 0.084 µm, corresponding to a mirror finish.

To demonstrate that the droplet condensation approach is viable for metals, liquid nitrogen was temporarily abandoned in exchange for a fluid that condenses at a more achievable temperature: water vapor. An FEI Quanta 200 environmental scanning electron microscope (ESEM) was set up using a small piece of the brass sample described above. The brass sample was placed on a cold stage within the ESEM, and the sample chamber was

pumped down to vacuum. Then the chamber was slowly refilled with environmental air. The reduced chamber pressure and chilled cold stage created psychometric conditions favorable to condensation of the water vapor that was mixed into the air. A representative water droplet, formed on the brass sample as a result of this process, is shown in Fig. 9. This droplet forms a static contact angle of 54.6° ± 5.6° with the brass.

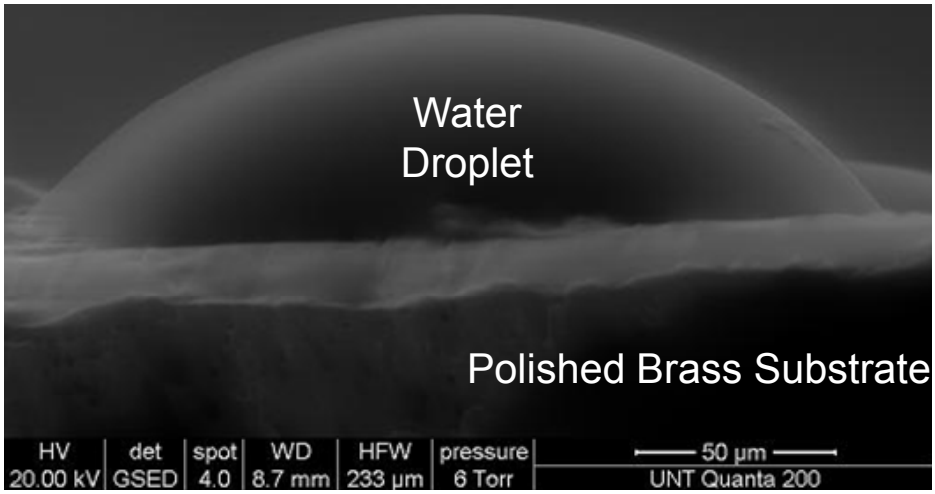

Figure 9. As a proof of concept for the droplet condensation approach to contact angle measurement, water droplets were formed on brass by condensation and imaged, all within an ESEM equipped with a cold stage.

V. Discussion

The apparatus to perform static sessile drop method measurements, shown in Fig. 5, was not successful in creating a viable droplet for contact angle measurement. While it might be possible to measure cryogenic liquid contact angles using the static sessile drop method, a much more sophisticated apparatus than the one shown in Fig. 5 is needed. A particular challenge will be accurately dispensing controlled liquid droplets from a hypodermic needle. A custom syringe, syringe pump, and tubing competent for remote operation at cryogenic temperatures in a sealed environment is needed.

The apparatus to perform droplet condensation method measurements, shown in Fig. 7, was also unsuccessful in creating a viable droplet for contact angle measurement because it was not insulated enough to achieve the required temperature. Of the two attempted approaches, the droplet condensation approach holds the most promise since it does not require a custom cryogenic syringe and syringe pump. The existing, non-functioning prototype apparatus informs design of a more sophisticated, functioning device, which will need to be environmentally insulated to achieve nitrogen condensation temperature while having optical access for a camera-equipped microscope.

As an intermediate step toward liquid nitrogen contact angle measurement, the droplet condensation method was successfully demonstrated for a metal surface by condensing water vapor to liquid. The measured contact angle, 54.6° ± 5.6°, is less than the accepted textbook value of 86.0°.[28] However, as pointed out by Gajewski,[29] static contact angles of liquids on brass go down as liquid volume is decreased. Thus, we expect to see a value lower than of 86.0° for a microscopic droplet. Moreover, the droplet contact angle may have been affected by the sample surface features illuminated in Fig. 8 since the scratches detected by profilometry are the same size as the droplet itself. Additional work with the ESEM can clarify the source of mismatch between the contact angle textbook value and the value measured for this micro-droplet via the condensation approach.

VI. Conclusions and Future Work

Orientation calculations show that for a range of evaporator temperatures from 300 K to 600 K the power-to-area ratio of a cryogenic Rankine cycle increases as the evaporator temperature gets hotter. This result confirms NASA's assertion that Rankine cycles can provide high power density and superior thermodynamic efficiency for future space missions compared to existing space-based energy generation methods. Moreover, for evaporator temperatures of 300 K and higher, the cryogenic Rankine cycle power-to-area ratio meets or exceeds the power-to-area ratio for PV arrays for condenser temperatures above 118 K. We have therefore shown that 1) two-phase

space-based cryogenic power cycles are thermodynamically feasible because condenser temperatures below the nitrogen critical point are accessible, enabling liquid production in the condenser and 2) space-based cryogenic Rankine cycles equivalent in area to PV arrays can produce more power. Thus, given that conventional PV arrays are routinely placed in orbit, viable cryogenic Rankine cycles are not too large to be put into space, as some critics have speculated.

The key to microgravity phase separation in a cryogenic Rankine cycle is harnessing liquid capillary effects to replace gravity for condenser phase separation. Under representative condenser conditions, a nitrogen gas self-diffusion coefficient of D_{N_2} = 6.33 10^{-10} m^2/s was calculated for the condenser. For a porous barrier made of capillaries 10 μm in diameter, the residence time under these conditions is 0.16 s. Given a particular mass flow rate and condenser diameter, this value indicates how thick a porous barrier must be to facilitate phase separation. Residence time for phase separation is an important cycle parameter because viscous losses and capillary forces within the porous barrier retard flow in the desired direction, requiring more pumping power to circulate fluid.

A microgravity Rankine cycle condenser containing a porous barrier for phase separation must maintain a pressure gradient within the condenser in excess of a normal Rankine cycle owing to Young-Laplace pressure. This space-based Rankine cycle will therefore have three distinct pressure zones, instead of the two major pressure zones found in terrestrial Rankine cycles.

A literature review of cryogenic contact angle measurements reveals that the seminal work in this field occurred in the 1970s with no modern follow-up work reported. Even the best 1970s studies were subject to uncertainties that can today be eliminated by modern, high-resolution digital photography and computational tools unavailable 30 years ago. An opportunity thus exists to update these early measurements for a range of relevant metal substrates and operating temperatures, and two different experimental attempts were made. The first, an adaptation of the static sessile drop method, was unsuccessful owing to the need for accurately dispensing controlled cryogenic liquid droplets from a hypodermic needle, the surface fouling from environmental contaminants, and the poor control of the stage temperature. The second approach, an adaptation of the droplet condensation method, was unsuccessful because cryogenic temperature required for condensation could not be achieved given poor insulation of the experiment from the environment. Nonetheless, the droplet condensation method was successfully demonstrated using water as a surrogate for nitrogen, and a contact angle of 54.6° ± 5.6° was measured on a polished brass sample using this approach.

Future work is planned that will use a commercially available cryogenic microscope stage, modified for visualization of droplet condensation, to reproduce with nitrogen the approach successfully demonstrated in Fig. 9 with water.

Acknowledgements

This work was supported by the Mechanical and Energy Engineering Department and the College of Engineering at the University of North Texas through the Researcher Incubator, a training organization to fast-track undergraduate students into engineering research experiences. The authors acknowledge Dr. Walid Aissa, a visiting scholar from the Department of Mechanical Power at the High Institute of Energy in Aswan, Egypt, for his assistance in creating the schematic representation of the droplet condensation contact angle apparatus. We also acknowledge Nelson Martinez, a doctoral student in UNT's Materials Science and Engineering Department, who provided Fig. 9.

References

[1] Lahey, R. T., and Dhir, V., "Research in Support of the Use of Rankine Cycle Energy Conversion Systems for Space Power and Propulsion," Report NASA/CR-2004-213142, 2004.

[2] Caillat, T., Borshchevsky, A., Fleurial, J., and Snyder, J., "Space Technology and Applications International Forum," Editor: El-Genk, M. S., American Institute of Physics, 2000.

[3] Lin, L., Yu, X.-L., Xin, Z., and Zhang, X.-Z., "Thermal Cycle Design of Liquid Nitrogen Engine," *Journal of Zhejiang University*, Vol. 40, No. 11, 2006, pp. 1989-1993.

[4] Plummer, M. C., Koehler, C. P., Flanders, D. R., Reidy, R. F., and Ordonez, C. A., "Cryogenic Heat Engine Experiment," *Advances in Cryogenic Engineering*, Vol. 43, 1998, pp. 1245-1252.

[5] Ordonez, C. A., and Plummer, M. C., "Experimental Car Which Uses Liquid Nitrogen as Its Fuel," *Proceedings of the Texas Section of the American Physical Society*, 1997, Houston, TX.

[6] Ordonez, C. A., Plummer, M. C., and Parker, M. E., "Experimental Results on the Operation of a Liquid Nitrogen-Based Cryogenic Heat Engine," *Bulletin of the American Physical Society Transactions B*, Vol. 41, 1996, p. 1857.

[7] Althausen, D. M., Quinn Jr., F. D., Bunnell, C. T., and Daidzic, N. E., "Porous Media Condensing Heat Exchanger with Integral Gas Liquid Separation for Space Flight Use," *Proceedings of the 44th AIAA Aerospace Sciences Meeting*, American Institute of Aeronautics and Astronautics Inc., Reston, VA, 2006, pp. 16186-16196.

[8] DiPirro, M. J., Boyle, R. F., Figueroa, O., Lindauer, D., McHugh, D. C., and Shirron, P. J., "Superfluid Helium Heat Transfer," *AIAA/ASME Thermophysics and Heat Transfer Conference*. Published by ASME, New York, 1990.

[9] DiPirro, M. J., and Zahniser, J., "Liquid/Vapor Phase Boundary in a Porous Plug," *Proceedings of the 1989 Cryogenic Engineering Conference*, Vol. 35, Part 1, 1990, pp. 173-180.

[10] Grigor, V. A., Pavlov, Y. M., and Ametistov, E. V., "Correlation of Experimental Data on Heat Exchange Accompanying Free-Volume Boiling of Some Cryogenic Liquids," *Teploenergetika*, No. 9, 1973, pp. 57-63.

[11] Stephan, K., and Abdelsalam, M., "Heat-Transfer Correlations for Natural Convection Boiling," *International Journal of Heat and Mass Transfer*, Vol. 23, No. 1, 1980, pp. 73-87.

[12] DiPirro, M. J., Boyle, R. F., Figueroa, O., Lindauer, D., McHugh, D. C., and Shirron, P. J., "The SHOOT Cryogenic System," *Superfluid Helium Heat Transfer*, United Engineering Center, New York, NY, 1990, p. 29,

[13] DiPirro, M. J., and Zahniser, J., "The Liquid/Vapor Phase Boundary in a Porous Plug," *Advances in Cryogenic Engineering*, Vol. 35, Plumum Press, New York, NY, 1990, pp. 173–180.

[14] Baranov, V. G., Vinnikov, A. I., and Gutkin, M. I., "A Study of the Operation of a Helium Vessel Phase Separator," Translated from *Khimicheskoe I Neftaynoe Mashinostroenie*, No. 8, August 1976, pp. 12–13.

[15] DiPirro, M. J., McHugh, D. C., and Zahniser, J., "Phase Separators for Normal and Superfluid Helium," *Proceedings of the Twelfth International Cryogenic Engineering Conference - ICEC 12*, 1988, pp. 681-689.

[16] Grigor, V. A., Pavlov, Y. M., and Ametistov, E. V., "Correlation of Experimental Data on Heat Exchange Accompanying Free-Volume Boiling of Some Cryogenic Liquids," *Teploenergetika*, No. 9, 1973, pp. 57-63.

[17] Brennan, P., and Skrabek, E., "Design and Development of Prototype Static Cryogenic Heat Transfer," Report NASA CR-121939, 1971.

[18] Bald, W. B., "Cryogenic Heat Transfer research at Oxford. I. Nucleate Pool Boiling," *Cryogenics*, Vol. 13, No. 8, 1973, pp. 457-69.

[19] Bland, M. E., "Bubble nucleation in cryogenic fluids," Ph.D. Dissertation, University of Oxford, June 1970.

[20] Steiner, D., and Schlunder, E. U., "Heat Transfer and Pressure Drop for Boiling Nitrogen Flowing in a Horizontal Tube, I. Saturated Flow Boiling," *Cryogenics*, Vol. 16, No. 7, 1976, pp. 387-98.

[21] NASA Mobile STS-119 Mission Update, "Second Part of Solar Array Deployment Complete", URL: http://portalforums.nasa.gov/mcs/mobile/index.jsp [cited 12 June 2009].

[22] Choi, B., Fuji, T., Asano, H., and Sugimoto, K., "A Study of Gas–Liquid Two-Phase Flow in a Horizontal Tube Under Microgravity," *Annals of the New York Academy of Sciences*, Vol. 974, 2002, pp 316-327.

[23] Narain, A., Kulkarni, S., Mitra, S., Kurita, J. H., and Kivisalu, M. T.,"Computational and Ground-Based Experimental Investigations of the Effects of Specified and Unspecified (Free) Pressure Conditions at the Condenser Exit for Condensing Flows in Terrestrial and Microgravity Environments," *Interdisciplinary Transport Phenomena: Annals of the New York Academy of Sciences*, Vol. 1161, 2009, pp. 321–360.

[24] Cussler, E. L., *Diffusion Mass Transfer in Fluid Systems*, 2nd Ed., Cambridge University Press, 1997.

[25] Lider, D. R., (Editor-In-Chief), "Mean Free Path and Related Properties of Gasses," *Handbook of Chemistry and Physics*, 87th Ed., CRC Press, Boca Raton, FL., p. 6.35.

[26] Washburn, E. W., "The Dynamics of Capillary Flow," Physical Review, Vol. 17, 1921, pp. 273-283.

[27] Deen, W. M., *Analysis of Transport Phenomenon*, Oxford University Press, 1998, p. 25.

[28] Collier, J. G., and Thome, J. R., Convective Boiling and Condensation, 3rd Ed., Oxford University Press, 142, 1976.

[29] Gajewski, A., "Contact angle and sessile drop diameter hysteresis on metal surfaces," *International Journal of Heat and Mass Transfer*, Vol. 51, No. 19-20, 2008, pp. 4628-4636.